# New approaches to nonlinear diffractive field propagation

P. Ted Christopher and Kevin J. Parker
*Department of Electrical Engineering and Rochester Center for Biomedical Ultrasound, University of Rochester, Rochester, New York 14627*

(Received 26 September 1989; revised 12 February; accepted 18 February 1991)

In many domains of acoustic field propagation, such as medical ultrasound imaging, lithotripsy shock treatment, and underwater sonar, a realistic calculation of beam patterns requires treatment of the effects of diffraction from finite sources. Also, the mechanisms of loss and nonlinear effects within the medium are typically nonnegligible. The combination of diffraction, attenuation, and nonlinear effects has been treated by a number of formulations and numerical techniques. A novel model that incrementally propagates the fields of baffled planar sources with substeps that account for the physics of diffraction, attenuation, and nonlinearity is presented. The model accounts for the effects of refraction and reflection (but not multiple reflections) in the case of propagation through multiple, parallel layers of fluid medium. An implementation of the model for axis symmetric sources has been developed. In one substep of the implementation, a new discrete Hankel transform is used with spatial transform techniques to propagate the field over a short distance with diffraction and attenuation. In the other substep, the temporal frequency domain solution to Burgers' equation is implemented to account for the nonlinear accretion and depletion of harmonics. This approach yields a computationally efficient procedure for calculating beam patterns from a baffled planar, axially symmetric source under conditions ranging from quasilinear through shock. The model is not restricted by the usual parabolic wave approximation and the field's directionality is explicitly accounted for at each point. Useage of a harmonic-limiting scheme allows the model to propagate some previously intractable high-intensity nonlinear fields. Results of the model are shown to be in excellent agreement with measurements performed on the nonlinear field of an unfocused 2.25-MHz piston source, even in the near field where the established parabolic wave approximation model fails. Next, the model is used to compare the water path and *in situ* fields of a medical ultrasound device. Finally, the model is used to calculate the spatial heating rate associated with a nonlinear field and to simulate the phenomenon of saturation-induced beam broadening.

PACS numbers: 43.25.Jh

## INTRODUCTION

There exist a number of theoretical approaches to the problem of plane, cylindrical, and spherical wave propagation in media with attenuation and nonlinearities. Important results and concepts can be found in references such as.[1-3] The earlier works have been extended to cases of focused or unfocused sources, where diffraction effects cannot be ignored. Treatments of focused sources, including the distortion of the waveform, focal gain, and focal width with respect to the small signal case, were examined in[4-6] and others. For unfocused beams, the far-field directivity in quasilinear through hard shock conditions was treated in Ref. 7, and the beam pattern of higher harmonics were shown to be related to the beam pattern of the fundamental and to the shock parameter. The formulation of Lockwood *et al.*[7] works well in qualitatively describing beam broadening and the growth of minor lobes of harmonics, although it did not account for the presence of "fingers" or higher harmonic sidelobes.

In the 1980s more extensive treatments have been coupled with numerical methods for solution of nonlinear distortion in unfocused near- and far-field regions, and focused fields. Collaborative efforts between groups in Norway (University of Bergen) and the U.S. (University of Texas, Austin) have used the parabolic approximation and a Fourier series expansion (frequency domain solution) to calculate sound fields from continuous, axially symmetric sources.[8,9] The parabolic approximation is useful for narrow beam profiles that vary slowly in the axial direction, and at some distance from the source. Focused sources were considered separately, also utilizing a parabolic approximation and small aperture angle and high *ka* (large aperture to wavelength ratio) assumptions.[10,11] The case of second harmonic generation under quasilinear conditions in Gaussian beams was described by Du and Breazeale,[12,13] who used the parabolic approximation and the method of successive approximations to derive analytic expressions. Bacon[14,15] considered the case of focused fields germane to medical imaging, and utilized numerical integration of equations also incorporating a parabolic approximation. Hamilton and Hart[16,17] furthered the earlier work[9] and used a parabolic approximation with a Fourier series approach that is solved by a backward finite difference algorithm applied to the set of coupled parabolic differential equations. The approach can incorporate a transformed coordinate system that is particularly useful for focused fields, and they have demonstrated fine detail in solutions, including the presence of higher harmonic "fingers" in the focal plane beam pattern.

We have employed an alternative approach to the general

 0001-4966/91/070488-12$00.80  

problem, in order to gain advantages in computational efficiency, to develop a formalism that does not require the parabolic approximation, and to allow for multiple layer propagations. Basically, our methodology utilizes an incremental propagation of an axially symmetric field from some plane at axial distance $z$ from the source to a parallel plane at distance $z + \Delta z$. The concept is illustrated in Fig. 1. The normal velocity radial profiles $u_1(z,r)$ of a fundamental (solid line) and higher harmonics $u_n(z,r)$ (dashed lines), $n = 2$ to $N$, are propagated together in $\Delta z$ steps. Note in Fig. 1 that to highlight the nonlinear effect over $\Delta z$, the initial field consists of the fundamental harmonic only.

First, the diffraction effect is accounted for by utilizing the (Fourier) convolution theorem and a discrete Hankel transform (DHT). The recently developed DHT[18] offers great computational savings[19] as compared to the two-dimensional discrete fast Fourier transform. Computing diffraction involves multiplying the DHT of each harmonic radial profile by its appropriate linear transfer function $H_n(z,R)$ [the DHT of the point spread function $h_n(z,r)$], which is equivalent to convolution in the original spatial domain, as implied by Huygen's principle. An inverse DHT gives the desired diffracted harmonic radial profile $u'_n(z + \Delta z,r)$ (the prime notation indicates intermediate results) for each harmonic present in the propagation. This diffraction operator is depicted in Fig. 2. Note also the presense of attenuation in the form of an attenuated transfer function. The nonlinear effect is accounted for by advancing the diffracted and discretely sampled field forward on a point-by-point basis over an equivalent incremental $\Delta z$ distance without diffraction, but with accretion and depletion of harmonics according to a temporal frequency domain solution to Burgers' equation (FDSBE).[20–22] That is, for some radial position $r_i$, the normal velocities $u'_n(z + \Delta z,r_i)$ are modified by nonlinear mechanisms to $u_n(z + \Delta z,r_i)$ as if the acoustic velocity represented a plane wave traveling in the direction of the phase front at $r_i$. This concept is illustrated in Fig. 3.

The model also accounts for the effects of refraction and reflection (but not multiple reflections) in the case of propagation through multiple, parallel layers of fluid medium.[19] The model's use of a novel harmonic-limiting scheme for the FDSBE[23] makes possible some previously intractable high-intensity (shocked) propagations. The model's approach appears to be a departure from other nonlinear models in its extensive use of transform (spatial and temporal) techniques. There are well-known computational advantages inherent in transform operations, but also pitfalls in implementations as discussed extensively in our companion paper on linear propagation.[19] These pitfalls can be avoided by appropriately windowing the point spread function $h$ or its transform $H$.

Conceptually, our approach is somewhat akin to the work of Pestorius and Blackstock,[24,25] who treated the nondiffracting propagation of plane waves in two domains using incremental advances. In the time domain, waveform distor-

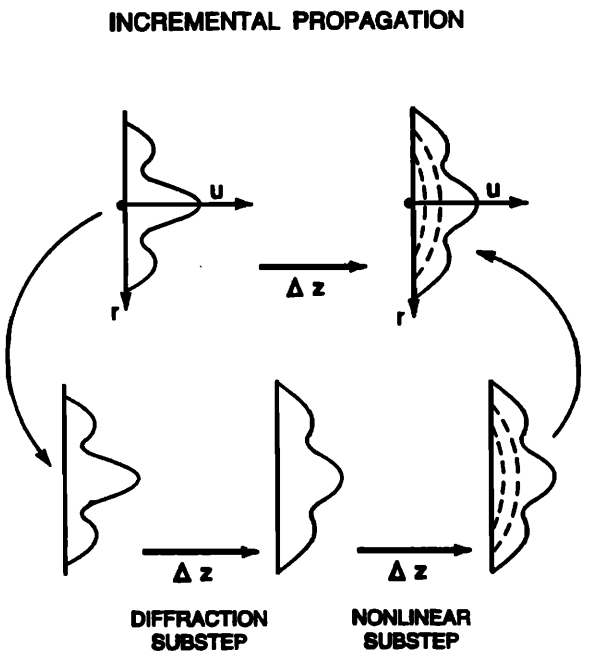


FIG. 1. Illustration depicting the concept of incremental field propagation using substeps for the diffraction and nonlinear operators. Shown are radial (transaxial) plots of normal velocity magnitude of the fundamental (solid lines) and the higher harmonics (dotted lines) at different stages in the propagation substeps. To highlight the nonlinear effect over $\Delta z$, the figure depicts an initial single harmonic field.

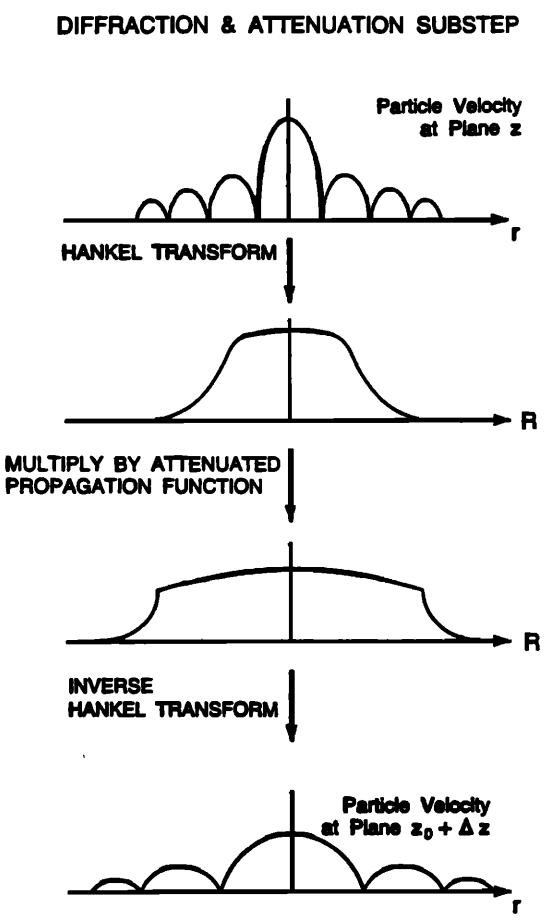


FIG. 2. The diffraction substep with its discrete Hankel transform useage (here applied to one harmonic using the RFSC approach).

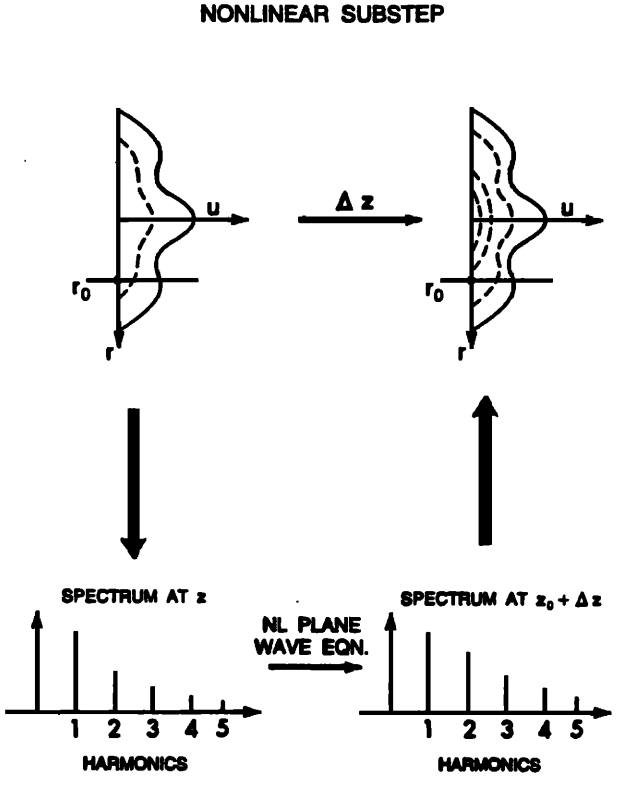


FIG. 3. The nonlinear substep with its FDSBE nonlinear plane-wave operator. The multiharmonic field at radial point $r_0$ is updated for nonlinear effects via the FDSBE algorithm.

tion over an increment was treated by accounting for the dependence of velocity on pressure. In the transform domain (temporal frequencies), the losses due to frequency-dependent attenuation were applied to the spectrum. In our scheme, nonlinear effects are accounted for in the temporal frequency domain via a Fourier series solution to Burgers' equation, and diffraction and attenuation are treated in the spatial transform (angular spectrum) domain. Despite these differences, the earlier work serves as a precedent in applying incremental effects within different domains.

## I. THE LINEAR DIFFRACTIVE SUBSTEP

Since the linear effects of diffraction, attenuation, refraction, and reflection are extensively covered in the companion paper,[19] the model's linear substep will only be summarized here. A multiharmonic, acoustic normal velocity (or pressure) field in a plane can be diffracted $\Delta z$ forward by convolving each of the constituent harmonic fields with an appropriate point spread function,

$$h_n(\Delta z,r) = -\frac{1}{2\pi}\frac{\Delta z}{d^2}\left(jnk-\frac{1}{d}\right)e^{jnkd}, \tag{1}$$

where $r$ is the radial coordinate, $n$ represents the harmonic index, and $d=\sqrt{r^2+\Delta z^2}$. Direct sampling of the $h_n(\Delta z,r)$ functions results in a correct implementation of the (Fourier) convolution theorem. Alternatively, convolution can be computed using direct sampling of the analytical Hankel transform of $h_n$,

$$H_n(\Delta z,R) = \begin{cases}\exp\left[j2\pi\Delta z\sqrt{(nf/c)^2-R^2}\right], & |R|\leqslant nf/c,\\ \exp\left[-2\pi\Delta z\sqrt{R^2-(nf/c)^2}\right], & |R|>nf/c.\end{cases} \tag{2}$$

An approach based on the sampling of $H_n(\Delta z,R)$ is computationally simpler since it doesn't require the discrete Hankel transforming of the $h_n$ functions. If nonaxis symmetric sources must be propagated, the model can be generalized to accomodate them by exchanging the current Hankel transform for a two dimensional FFT.

While analytically a repeated convolution over many $\Delta z$ increments is straightforward, the use of discrete, finite length (spatial) transforms requires some modification to avoid convolutional artifacts. This involves "windowing" and sampling issues in the spatial and transform domains and is explored in the companion paper.[19] Frequency-dependent attenuation can be included in the diffractive substep, by either including a loss term with the point spread function $h_n$, or by using a ray theory interpretation to account for losses in the transform function, $H_n$.[19]

Refraction and reflection (but not multiple reflections) at parallel fluid boundaries can be accounted for in the $H_n$-based diffraction (RFSC) substep. Using the angular spectrum interpretation of $H_n$, the problem can be simplified to the treatment of plane waves. The integration of the complex analytical transmission coefficient for a plane wave into the RFSC multistep propagation scheme is presented in detail in Ref. 19. The computational cost of the inclusion of the attenuation, refraction, and reflection operators with the diffraction substep is neglible.

## II. THE NONLINEAR SUBSTEP

In general, the acoustic normal velocity field at a point $r_i$ in a plane given by $z_i$ can be represented by a multiharmonic waveform (even if the source is pulsed). If this normal velocity waveform represented a plane wave traveling in the $z$ direction, then the effect of nonlinearity on the waveform in traveling over a distance $\Delta z$ could be computed using the frequency domain solution to Burgers' equation (the attenuation term of the FDSBE is not considered here as attenuation is computed in the linear diffractive substep of our model). In this way, the model accounts for the nonlinear effect by supplementing each $\Delta z$ linear substep with a $\Delta z$ nonlinear plane-wave advancement of the field. The resulting two substep, nonlinear $\Delta z$ advancement of the field is depicted in Figs. 1–3. The order of the substeps is reversible, but hereafter for discussion purposes will be assumed to be, linear first, nonlinear second.

The nonlinear plane-wave substep then consists of applying the FDSBE (minus the attenuation term) to each multiharmonic radial field sample that has been output by the most recent linear substep. The $i$th iteration of the FDSBE algorithm can be written

$$u_n(z+\Delta z,i) = u'_n(z+\Delta z,i) + j\frac{\beta\pi f\Delta z}{2c^2}\left(\sum_{k=1}^{n-1} k u'_k u'_{n-k} + \sum_{k=n}^{N} n u'_k u'^{*}_{k-n}\right), \quad n=1,2,\ldots,N, \tag{3}$$

where $\beta$ is the nonlinear parameter $1 + (1/2)B/A$, $f$ is the fundamental frequency, and $u_n(z + \Delta z,i)$ denotes the $n$th term in an $N$ term complex Fourier series describing the temporal normal velocity waveform at the $i$th radial field sample in the plane $z + \Delta z$. Note that in the bracketed summation terms the $u'_k(z + \Delta z,i)$ terms have been abbreviated by dropping the $(z + \Delta z,i)$ designation. This computation is repeated for each of the N radial samples ($i = 0,1,...,N - 1$). The first summation in large parentheses represents the accretion of the $n$th harmonic by nonlinear combination of other harmonics that have a sum frequency of $nf$. The second summation, with conjugation, can be interpreted as a depletion of the $n$th harmonic to other harmonics with a difference frequency of $nf$.

To better account for wave or phase front curvature within the nonlinear substep, correction terms have been added where $\Delta z$ is replaced by $\Delta z/\cos\theta[u_1(z,i)]$ and $u_n(z,i)$ is replaced by $u_n(z,i)/\cos\theta[u_1(z,i)]$ to account for the direction and magnitude of the actual (not normal) field at radial point $i$. Also, $\theta[u_1(z,i)]$ is the angle that the phase front of the fundamental harmonic at the point $(z,r_i)$ makes with respect to the $z$ axis. This angle (hereafter referred to as the directionality) is obtained by calculating the rate of change of phase of the fundamental with respect to radial distance:

$$\theta[u_1(z,i)] = \frac{d}{dr}\left[\tan^{-1}\left(\frac{\mathrm{Im}[u_1(z,r)]}{\mathrm{Re}[u_1(z,r)]}\right)\right]_{r=r_i}. \quad (4)$$

Thus, the model assumes that at each radial point, the phase fronts of the harmonics all have the same directionality as the fundamental. The assumption that all harmonics travel together in the same direction (at any given radial point) is implicitly required by the use of the nonlinear plane-wave equation. Actually, calculations and comparisons of the directionalities of the first four harmonics have shown this assumption of the consistency of the directionalities of the different harmonics is only loosely justified—at any given radial point in a given plane the different harmonics have small differences in their phase front directionalities (this will be the subject of a later report). Note that the model's explicit inclusion of the field's local directionality is in contrast to the established parabolic wave model's[9,16] implicit assumption that the directionality is consistent with the computational coordinates. This implicit assumption is valid only for the simple, nondiffracting cases (plane, cylindrical, and spherical waves) with the obvious coordinate systems.

One serious shortcoming of the frequency domain solution to Burgers' equation (FDSBE) is the large number of harmonics required to propagate shockwaves. (This problem is also encountered in the comparable established time domain solutions, as they also require the frequency domain to represent medium attenuation.) When the shock front discontinuities are large and steep—as routinely occurs with high intensity fields in lightly attenuating fluids—then the number of harmonics required to represent the discontinuities can be in the hundreds or even thousands. In terms of the number of harmonics $N$, the computational complexity of the single step of the FDSBE is of order $N^2$. Additionally, the step size requirements drop roughly in proportion to $N$, thus making the overall complexity of the FDSBE-based nonlinear (plane-wave) propagation approximately $N^3$ (Ref. 23). Combining this with the $N^2$ complexity of the DHT-based single-step diffraction operators[19] ($N^2$, since the number of radial samples N needed rises roughly in proportion to $N$), this gives an $N^5$ computational complexity to our nonlinear diffraction model. Consequently, there is a great need to limit $N$ and still maintain good accuracy.

An approach to limiting the number of harmonics used in the FDSBE operator has been found that works well with initially sinusoidal sources.[23] The approach involves implicitly limiting the steepness of the shockfronts formed by artificially ramping up the medium's attenuation function. Specifically, the exponential attenuation constant $b$ is replaced by the function

$$b(n) = b + [(n - 1)/N] * q, \quad (5)$$

where $q$ is a constant describing the exponential ramping of the medium attenuation function. This scheme has proven to be accurate and relatively insensitive to variations in $q$ for propagating continuous plane waves, with the only harmonic distortion produced appearing in the highest harmonics included in the propagation (as well as those not included, which are implicitly assigned zero amplitude). The approach should then allow for accurate modeling of nonlinear continuous diffractive fields since the only additional error should be attributable to differential diffraction effects (between the harmonic-limited scheme and a very large, or ideally infinite, harmonic scheme) and very little energy is found in the highest harmonics. The harmonic-limited scheme greatly simplifies, and in some cases makes tractable, the nonlinear propagation of high-intensity sinusoidal sources. For very large amplitude sinusoidal sources involving near-field shocks though, even this harmonic-limited scheme can require excessive harmonics (harmonic requirements rise rapidly to insure the stability of the waveform artifacts associated with a nonzero $q$ under the strong effects of near-field diffraction). In this case, and for the case of nonlinear pulse propagation, a much more stable limited-harmonic nonlinear algorithm has been developed in the time domain.

## III. CALCULATION OF THE SPATIAL HEATING RATE

The two substep, incremental nonlinear advancement of a diffractive field can be modified to permit the computation of the temporal average heating rate associated with the absorption of the propagating field. The modification involves treating the field as plane wavelike in the immediate vicinity of any given point (as is done with the nonlinear substep) and thus estimating the heating rate as the divergence of the intensity.[26] The multiharmonic field at any point can, using the impedance relation and the directionality, be converted into values of the average acoustic intensity, $I_n$, $n = 1,2,...,N$, where $I_n = (\rho c/2)(|u_n|^2/\cos^2\theta)$ is the temporal average intensity of the $n$th harmonic component at the point. The corresponding spatial heating rate can then be computed as

$$S = \sum_{n=1}^{N} 2I_n \alpha (nf)^{b(n)}, \tag{6}$$

where the modified power law relation for attenuation (5) is used.

## IV. COMPUTATIONAL ISSUES

Several different implementations of the nonlinear field propagation model have been developed. Of these, the most general and practical implementation developed for multilayer medium propagation will be discussed. This model uses the very efficient RFSC multistep diffraction operator exclusively. The resulting algorithm is simply a multistep RFSC linear propagation algorithm (as presented in Ref. 19) with a nonlinear substep applied between each RFSC linear substep. To simplify the computation the model allows for a specified radial tapering of the field of nonlinear computation. This tapering can be based on a linear propagation of the field to determine where the field amplitudes are sufficiently large to involve nonlinear effects. Also, the model allows the propagation to be partitioned into several different regions, each with its own medium parameters and propagation parameters. Each region is specified by a starting and ending $z$ coordinate.

The propagation parameters for any given region include the axial step size $\Delta z$ and the maximum number of harmonics $N_{\max}$. The reason a maximum harmonic is specified is that the model adds harmonics dynamically as required using a simple algorithm based on the amplitudes of the highest harmonic currently included in the propagation. The maximum number of harmonics should be large enough to accurately describe the anticipated nonlinear effects. The size of the nonlinear effects can be estimated by inputting the maximum linear field propagation amplitudes found in a region into the FDSBE. In general, if no shocks are anticipated then five to ten harmonics can adequately describe a continuous wave field. On the other hand, if shockwaves are expected then 30 to 50 harmonics and possibly a nonzero excess attenuation parameter $q$ (if the amplitudes are quite large and/or the absorption is small) will be required.

The selection of a $\Delta z$ step size for a region is based on an accurate accounting of the effects of diffraction, absorption, and nonlinear growth on the propagating harmonics. If the near-field region is not of excessively high amplitudes then a $\Delta z$ small enough to clearly display the axial variations of the fundamental frequency (except in the extreme near field) is adequate in describing the nonlinear growth of the field's higher harmonics. In the focal or far-field region of a high-amplitude device the selection of $\Delta z$ should be based on the accurate accounting for of the attenuation and nonlinear growth of the highest harmonic. A rule for selecting $\Delta z$ in such a region is to choose it small enough such that the resultant exponential attenuation across $\Delta z$ for the highest harmonic is no smaller than 0.7. A step size small enough to meet this criteria insures the accuracy of the nonlinear operator (3). Such a $\Delta z$ has accurately described the joint effect of nonlinearity and attenuation in one dimensional propagation[23] and diffractive propagation.

The radial sampling rate of the field should be large enough to describe the significant spatial frequency content of the highest harmonic included in the propagation. For focused field propagations involving up to 50 harmonics, a radial sampling rate of $4\times$ the Nyquist rate of the fundamental has given very good results. For unfocused fields, 1 or $2\times$ the Nyquist rate of the fundamental has worked very well. Confirmation of the adequacy of the sampling rate is obtained by examining the radial profiles of the highest harmonics. If the radial sampling rate is too small, then these profiles will, in their radial extent, prematurely lose coherence (before the limited precision of the numerical representation dictates).

To reduce the time requirements of the diffraction operator multiple (embedded) transform tables are utilized. Thus instead of using one large $Y(i,m)$ table with an N and a $T$ large enough for the fundamental harmonic for all the other harmonics, two smaller tables are added to simplify the transforming of the higher harmonics. These tables utilize smaller N's and $T$'s appropriate to the reduced radial extents of the higher harmonics (but which have the same radial spatial samples as the fundamental's over their reduced radial extent).

## V. EXAMPLES

Du and Breazeale[13] measured and predicted the finite amplitude pressure field of an unfocused 2-MHz Gaussian transducer operating in water under quasilinear conditions. Their prediction was based on analytical expressions derived using the parabolic approximation and the method of successive approximations. Their axial field predictions and measurements for the fundamental and second harmonic amplitude are shown in Fig. 4(a). Note the scaling of the second harmonic ($\times 100$) and the discrepancy between the prediction amplitudes that cross at about 20 cm and the measurement points which do not. The corresponding results obtained with our model are depicted in Fig. 4(b). Our calculation used six harmonics and the normal velocity output was converted to pressure output using the impedance relation. The agreement between the corresponding predicted results is good. The radial harmonic amplitudes at $z = 15$ cm for the fundamental and second harmonic as measured and predicted by Du and Breazeale are shown in Fig. 5(a). Both harmonics have been normalized to have an on-axis amplitude of 1. The corresponding results predicted by our model are displayed in Fig. 5(b). Also shown are the third and fourth harmonic amplitudes. The agreement between our model results and Du and Breazeale's measurement and theory is good. The agreement between the results is not surprising because the parabolic approximation should accurately describe an unfocused Gaussian beam.

Baker *et al.*[27] measured and predicted (using the parabolic approximation model) the nonlinear pressure field of an unfocused, plane circular piston source operating in water. The source had an initial frequency of 2.25 MHz, an initial amplitude of 100 kPa, and a radius of 19 mm. The measured axial harmonic amplitudes for the first three harmonics are shown for the first 750 mm of propagation in Fig. 6(a). The

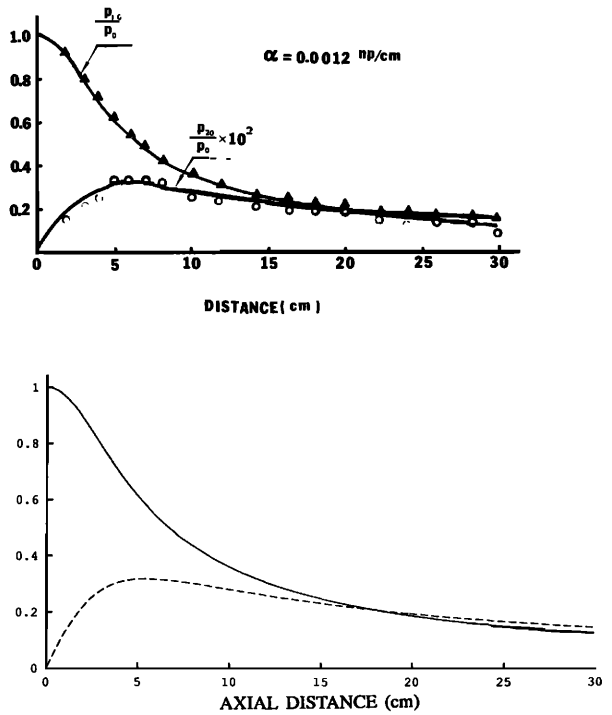


FIG. 4. Comparison with the measured and computed, unfocused Gaussian, axial harmonic pressure amplitudes of Du and Breazeale (1985). (a) Their axial results, note the scaling of the second harmonic. (b) Our computed results (using the same scaling).

corresponding results from our model (using 50 harmonics) are shown in Fig. 6(b). The model's normal velocity output has been converted to pressure using the impedance relation. Baker *et al.*'s log scaled second and third harmonic amplitudes, as measured and predicted, are shown in Figs. 7(a)

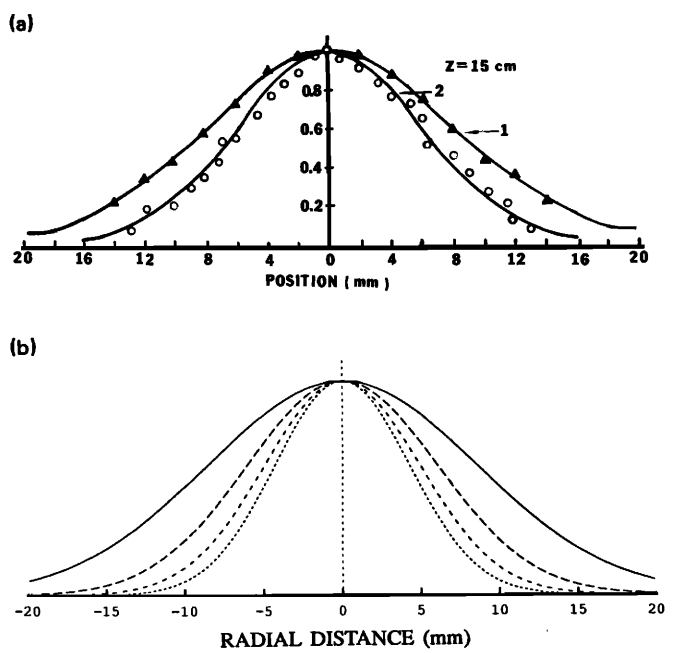


FIG. 5. Comparison with the measured and computed unfocused Gaussian radial beam patterns of Du and Breazeale (1985). (a) Their linearly scaled radial results at $z = 15$ cm. (b) Our corresponding results for the first four harmonics.

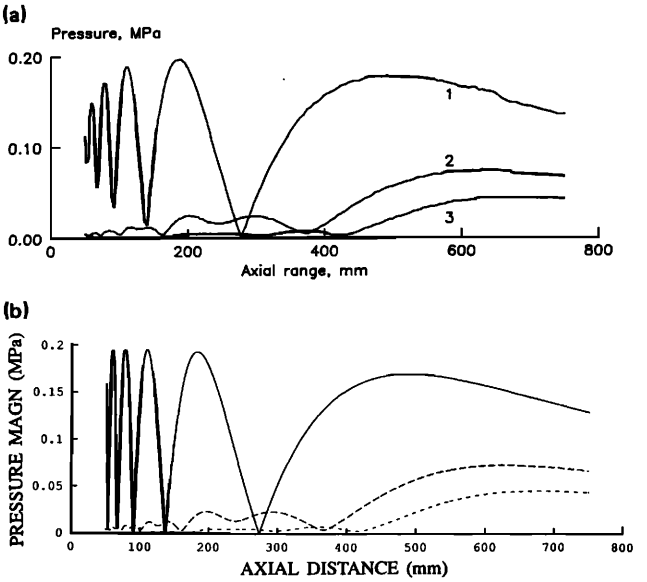


FIG. 6. Comparison with the measured axial harmonic pressure amplitudes of Baker *et al.* for an unfocused 2.25-MHz piston transducer. (a) First three measured harmonic amplitudes. (b) Corresponding computed results from our model.

and 8(a), respectively. The near-field errors in their predicted second and third harmonic amplitudes are consistent with the limitations of the parabolic approximation.[27] Figures 7(b) and 8(b) display the corresponding predictions of

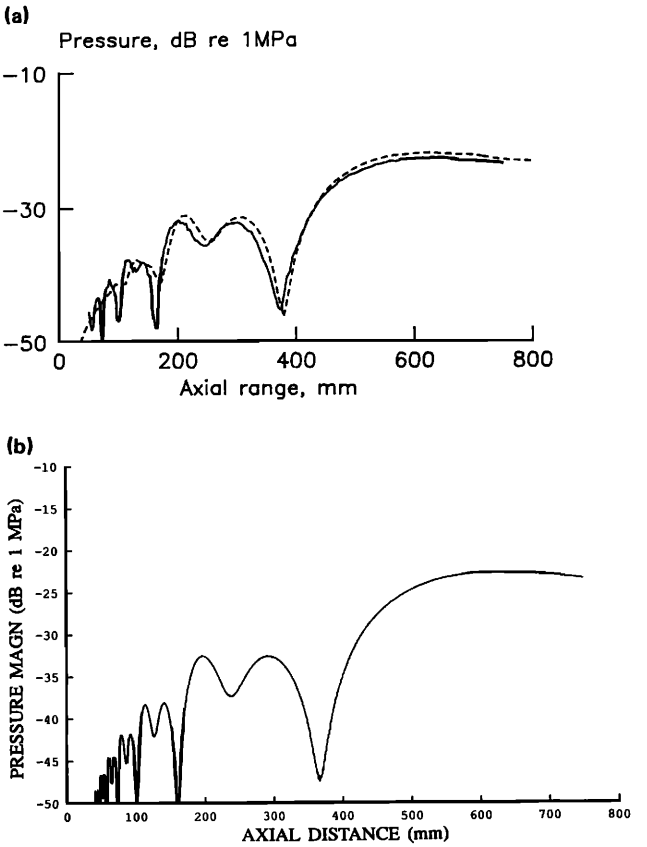


FIG. 7. Comparison with the log scaled, measured, and computed (using the parabolic approximation model), second harmonic axial amplitude of Baker *et al.* (a) Their measured and predicted results (solid line is measured). (b) Our corresponding computed result. Note the difference between the near-field computed results.

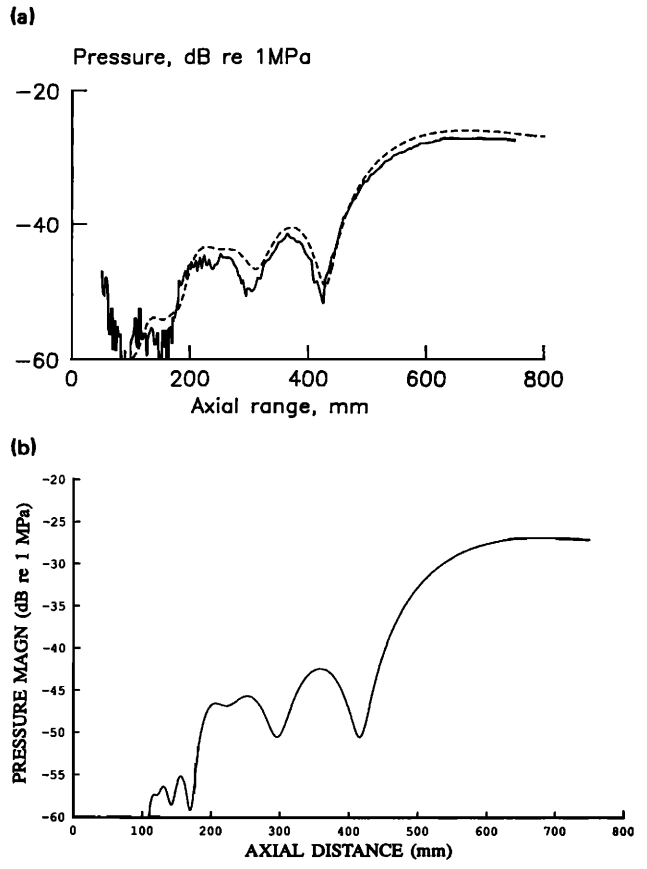


FIG. 8. Comparison with the log scaled, measured, and computed third harmonic axial amplitude of Baker *et al.* (a) Their measured and predicted results (solid line is measured). (b) Our corresponding computed result.

our nonlinear propagation model. The computed results agree with the measurements in the near field and the far field. The far-field agreement is best seen in comparing Fig. 6(a) and (b). The model's near-field results are visibly in close agreement with the measured values even when the parabolic approximation model fails. Note the molar like structure between 100 and 160 mm in the measured second harmonic axial result of Fig. 7(a) and the corresponding structure in the model computed result of Fig. 7(b). The small discrepancy in the near-field nodal depths of our predicted second harmonic result and their measured result could be due to the limitations of measuring the near field with a 1-mm diameter membrane hydrophone.

Figure 9(a) depicts the measured and predicted radial harmonic pressure profile of Baker *et al.*, at an axial distance of 275 mm. This axial distance corresponds to the location of the last axial minimum of the fundamental. Figure 9(b) shows the corresponding results computed using our model. The normal velocity output of the model was again converted to pressure using the impedance relation (as a check the Rayleigh integral[19] was also used but gave the same result). One interesting difference between the computed results of both models and the corresponding measured results is the drop off rate of the second and third harmonic profiles. The computed results roughly agree with each other, but they show a steeper drop off rate in harmonic amplitude than was measured. Baker *et al.* suggest that the limitations of the parabolic approximation, combined with the low signal levels off-axis, explain the off-axis difference between their measured and computed second and third harmonic amplitude curves. Our model should perform as accurately at these off-

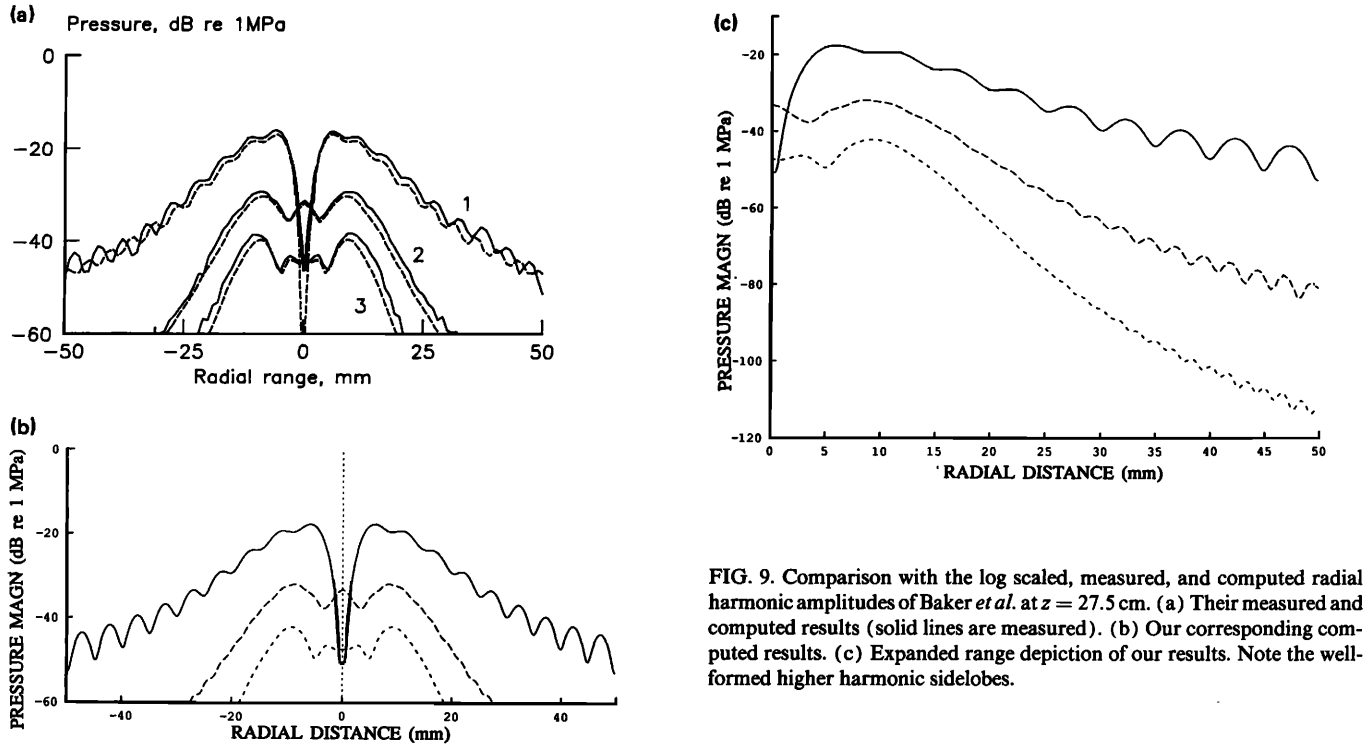


FIG. 9. Comparison with the log scaled, measured, and computed radial harmonic amplitudes of Baker *et al.* at $z = 27.5$ cm. (a) Their measured and computed results (solid lines are measured). (b) Our corresponding computed results. (c) Expanded range depiction of our results. Note the well-formed higher harmonic sidelobes.

axis radial distances as on-axis. In both cases, the computed directionalities of the fundamental and higher harmonics were parallel to the $z$ axis over the radial range of interest and thus no differential directionalities amongst the harmonics existed (which is not accounted for in our model). Figure 9(c) is an expanded depiction of the computed results shown in Fig. 9(b). Note the well formed sidelobes of the second and third harmonics.

In the companion linear paper,[19] the field of a 3-MHz focused piston source operating in a water medium and in a layered fat/liver, biomedical imaging medium was considered [see Fig. 9(a) and (b)]. The water medium had parameters $c = 1500$ m/s, $\rho = 1.0$ g/cm$^3$, $\alpha = 0.00025$ Np/cm, and $b = 2$. The two-layer medium consisted of 2 cm of fat with parameters $c = 1460$ m/s, $\rho = 0.95$ g/cm$^3$, $\alpha = 0.15$ Np/cm, and $b = 1$, followed by 10 cm of liver with parameters $c = 1570$ m/s, $\rho = 1.05$ g/cm$^3$, $\alpha = 0.03$ Np/cm, and

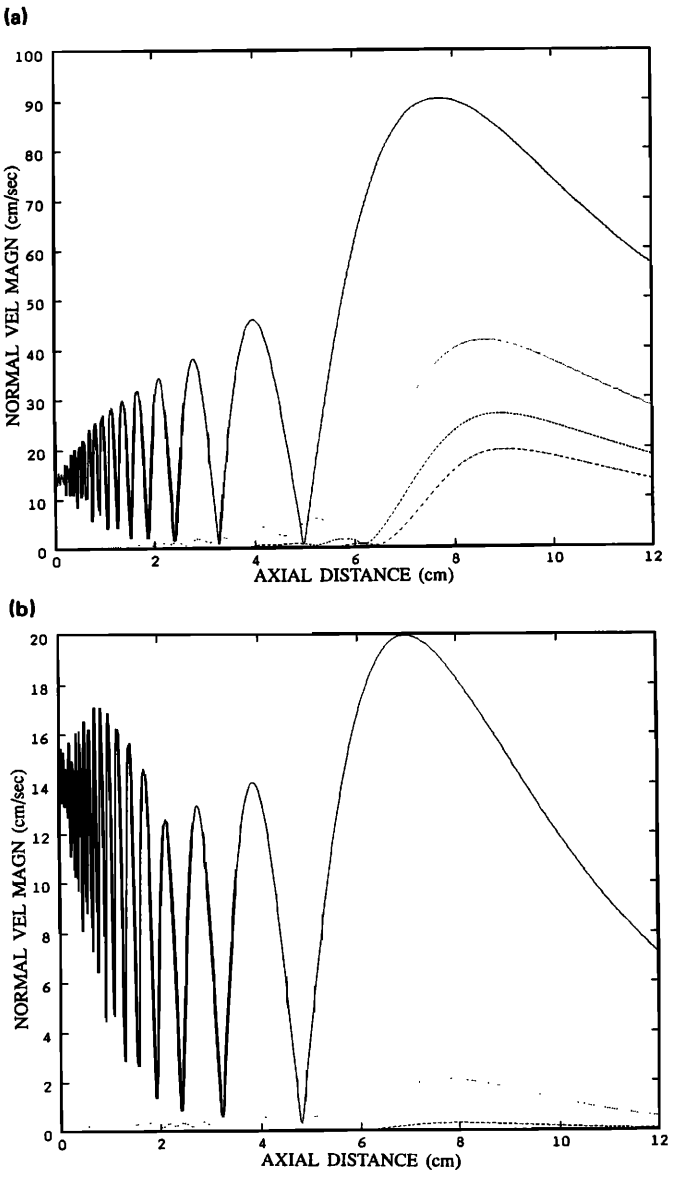


FIG. 10. Axial harmonic normal velocity amplitudes for a 3-MHz focused piston transducer. The peak source intensity is 3 W/cm$^2$. First four harmonics shown. (a) Water propagation. (b) Fat/liver propagation (2 cm of fat followed by 10 cm of liver).

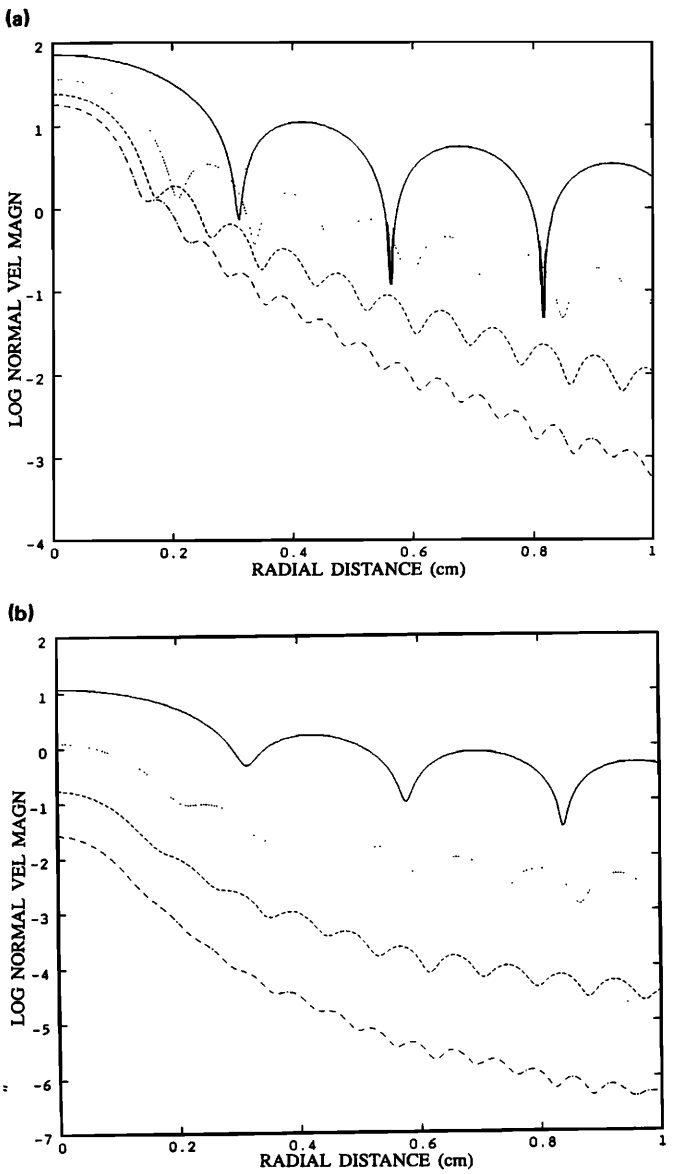


FIG. 11. Radial harmonic amplitudes for the focal plane of the 3-MHz focused piston transducer considered in Fig. 10. First four harmonics shown log scaled. (a) Water propagation. (b) Fat/liver propagation.

$b = 1.3$.[28,29] The transducer had a geometric focal length ($F$) of 10 cm, a radius of 1 cm, and an initial source peak intensity of 0.1 W/cm$^2$. The focusing was accomplished by applying a spherically focusing phase factor ($e^{j\theta(r)}$, where $\theta(r) = (2\pi f/c)\sqrt{r^2 + F^2}$) on the source plane amplitudes. By increasing the source intensity of the transducer to 3.0 W/cm$^2$, the resulting fields show significant nonlinear effects. Our nonlinear model was used to compute these resulting fields, and in particular, to gain insight into the actual fields produced by such medical devices in imaging the body at these intensities.

The nonlinear parameters $\beta$ used in modeling the three mediums were 3.5 for water, 4.7 for liver, and 6.5 for fat.[30] The model's axial results for the two cases are shown in Fig. 10(a) and (b), in the form of the first four harmonic amplitudes. The amplitudes shown in this example represent the normal velocity component of the acoustic field (the stan-

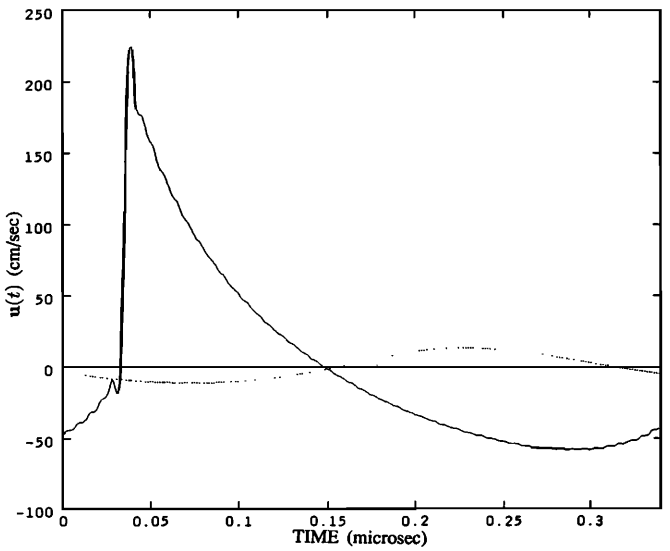


FIG. 12. Overlay of the time waveforms for the 3-MHz focused piston transducer of Fig. 10 taken at the focal point. The water propagation case is the solid (shocked) waveform. The fat/liver propagation case is the dotted (nearly sinusoidal) waveform.

dard input and output to the model). The corresponding radial focal plane harmonic amplitudes are depicted in Fig. 11(a) and (b). These results show a marked decrease in the amount of nonlinear distortion present in the fat/liver biological imaging medium, in spite of the larger nonlinear constants for these materials. This reduction is due to the increased absorption of the biological medium that results in greatly reduced focal wave amplitudes. These reduced amplitudes, as well as the reduced nonlinear distortion, can be seen clearly in the overlay of the corresponding focal time waveforms shown in Fig. 12. The water propagation utilized the specified limit of 50 harmonics, while the fat/liver propagation utilized only 8 harmonics. An excess attenuation factor $q$ of 0.35 was necessary to obtain the water results. The use of this excess attenuation factor results in a small and predictable perturbation in the computed focal shock waveforms. This perturbation can be seen as the ripple at the base and top of the shockfront of the water focal waveform in Fig. 12. These results suggest that in the ultrasound imaging of tissue such as liver the nonlinear field effects are much smaller than in the corresponding measurement medium (water). Future runs with the model in other biological imaging tissue and with other focused sources should provide insight into the possible nonlinear field effects associated with commercial biomedical ultrasonic imaging devices.

One nonlinear acoustic phenomena that has received attention recently as a possible source of bio-effects, and as a possible treatment for tumors, is nonlinear enhanced tissue heating. The absorption of any acoustic wave is frequency dependent. The higher the frequency content of the wave, the faster it is absorbed. Because nonlinearity continuously transforms low-frequency energy to higher frequency energy it accelerates the absorption of any acoustic wave. One outstanding example of this phenomenon occurs when an intense nonlinear focal field forms in a lightly attenuating medium and then enters a strongly attenuating medium. As

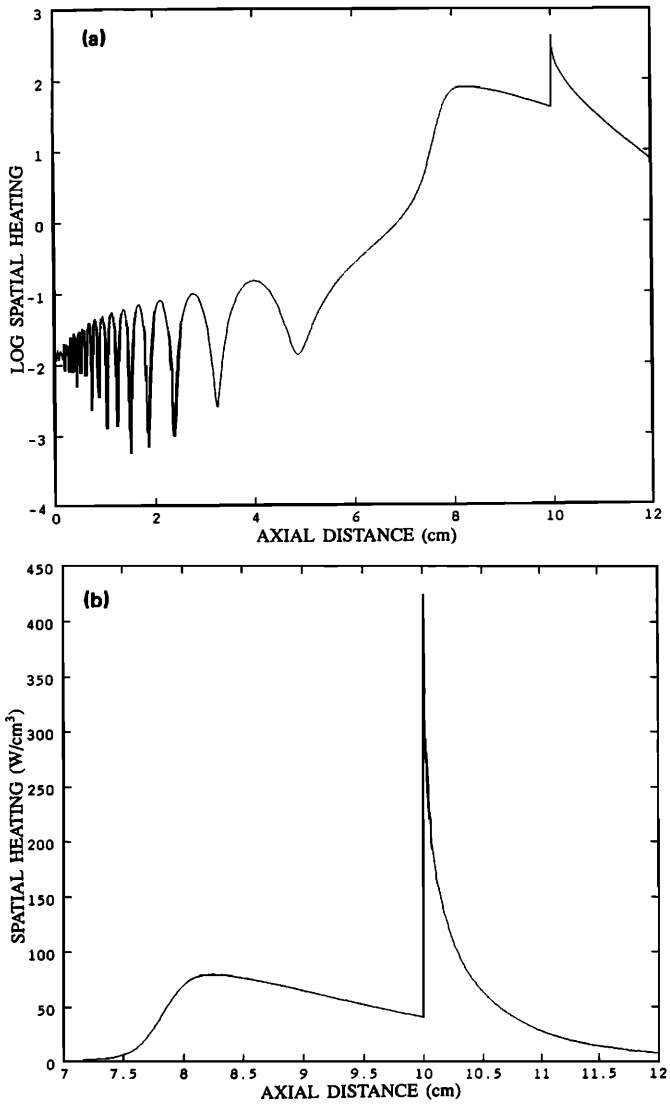


FIG. 13. Axial spatial heating rate for a 3-MHz focused piston transducer. The peak source intensity is 6 W/cm$^2$. The medium consists of 10 cm of water followed by 2 cm of fat. (a) Log scaled result. (b) Linear scaled result in the focal region (7–12 cm). The jump at the water/fat boundary is from 41–425 W/cm$^3$.

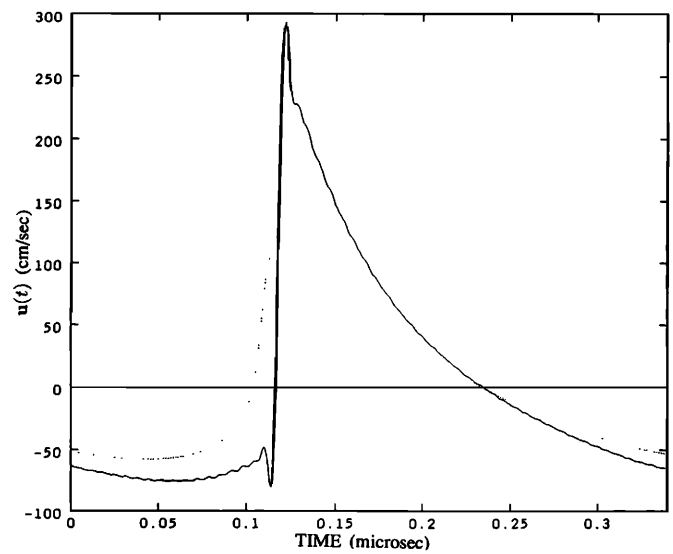


FIG. 14. Overlay of the axial waveforms for the piston transducer of Fig. 13 from z = 9.9 cm (in water, solid line) and z = 10.5 cm (in fat).

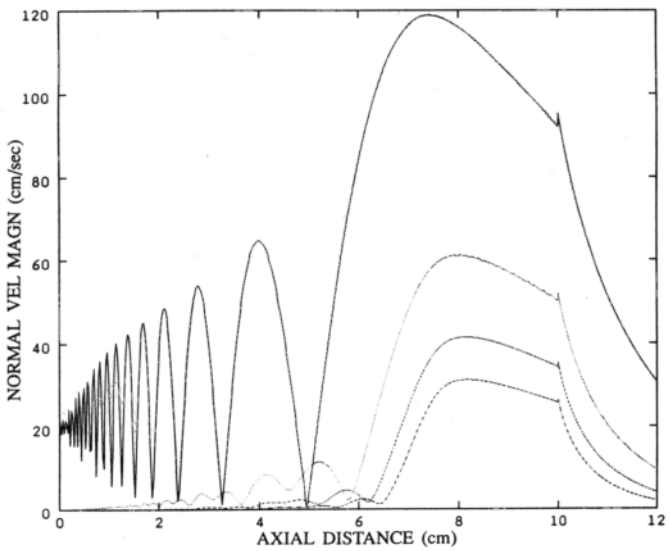


FIG. 15. Axial harmonic normal velocity amplitudes for a 3 MHz focused piston transducer of Fig. 13. First four harmonics shown. Note the rapid losses in the fat layer (after a small increase due to the difference in sound speed and density between the two media).

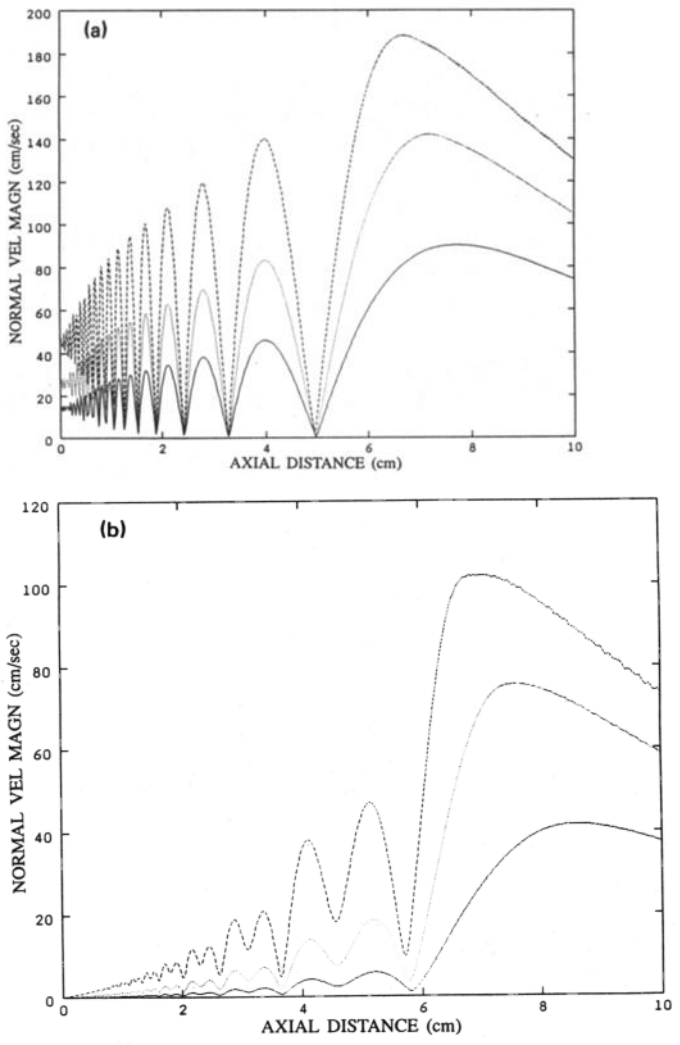


FIG. 16. Fundamental and second harmonic axial normal velocity amplitudes for the previously considered 3-MHz focused piston transducer operating at 3, 10, and 30 W/cm$^2$. (a) Overlay of the fundamental harmonic amplitudes. (b) Overlay of the corresponding second harmonic amplitudes.

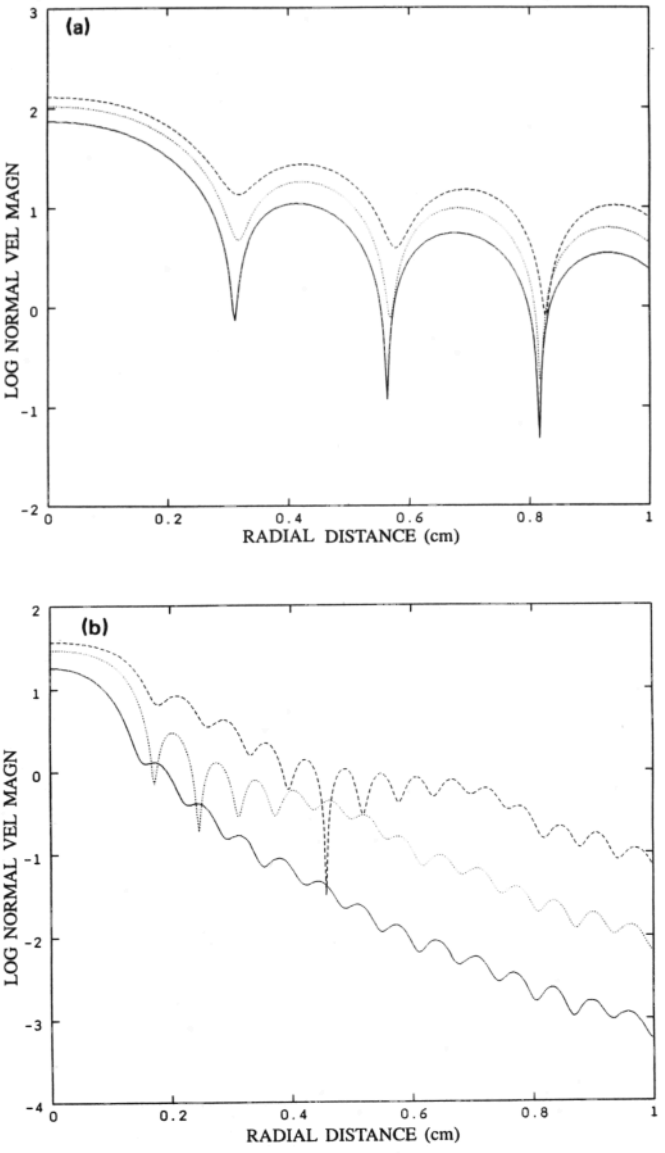


FIG. 17. Fundamental and fourth harmonic focal plane radial amplitudes for the 3-MHz focused piston transducer operating at 3, 10, and 30 W/cm$^2$. (a) Overlay of the fundamental harmonic profiles. Note the shift and loss in depth of the nodes associated with increasing source amplitudes. (b) Overlay of the fourth harmonic profiles. Note the broadening of the main lobes and the "shoulders" visible at 10 and 30 W/cm$^2$.

the field enters the highly absorbing medium, it is rapidly attenuated producing a region of high acoustic heating. An example of this phenomenon is displayed in Figs. 13–15. Here, the previously described 3-MHz focused transducer is operated at a source intensity of 6 W/cm$^2$ with an initial medium of water and a subsequent absorbing layer of fat. The water/fat boundary plane is located at the geometric focal distance of 10 cm. Fifty harmonics and an excess attenuation factor $q$ of 0.5 were used. Figure 13(a) and (b) show the computed axial heating rate in W/cm$^3$ associated with the attenuation of the field. Figure 13(a) is log scaled, while (b) linearly depicts the results in the focal region (7–12 cm). The axial heating rate jumps from 41–425 W/cm$^3$ at the boundary between the two mediums. Also, note the rapid increase in the heating rate starting at 7.5 cm (in water) due

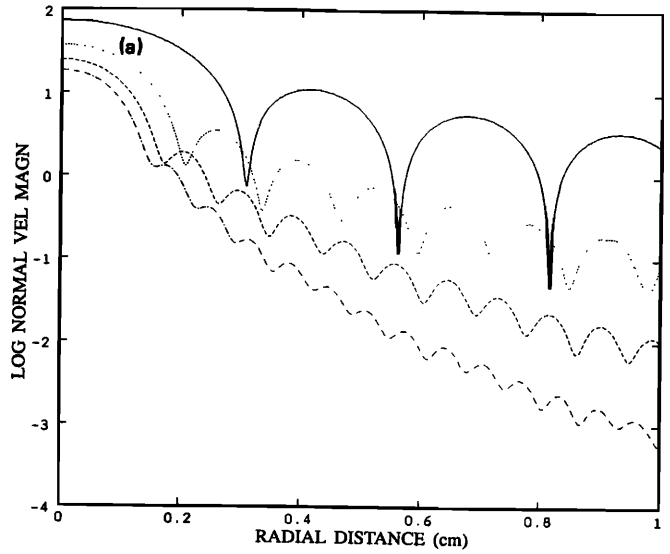


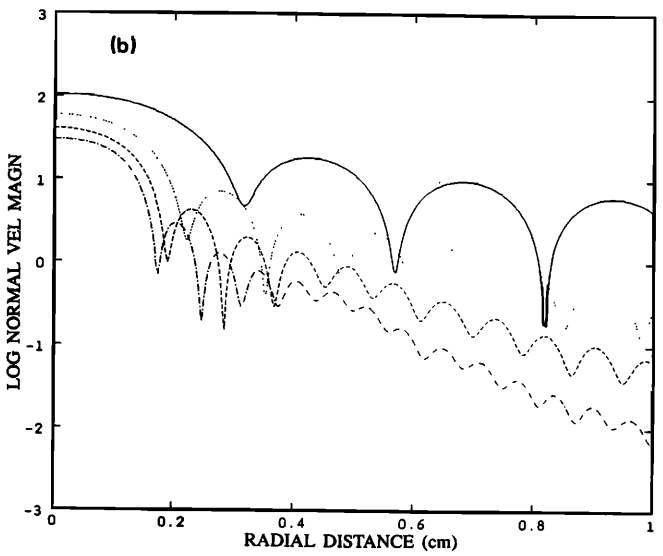


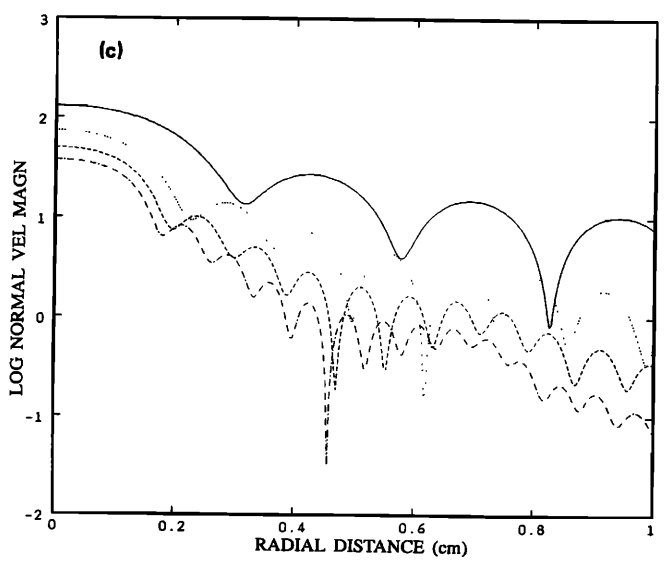


FIG. 18. First four harmonic amplitude profiles at the focal plane for the 3-, 10-, and 30-W/cm$^2$ field propagations. (a) Harmonic radial profiles for the 3-W/cm$^2$ source amplitude case. (b) Harmonic radial profiles for the 10-W/cm$^2$ case. (c) Harmonic radial profiles for the 30-W/cm$^2$ case.

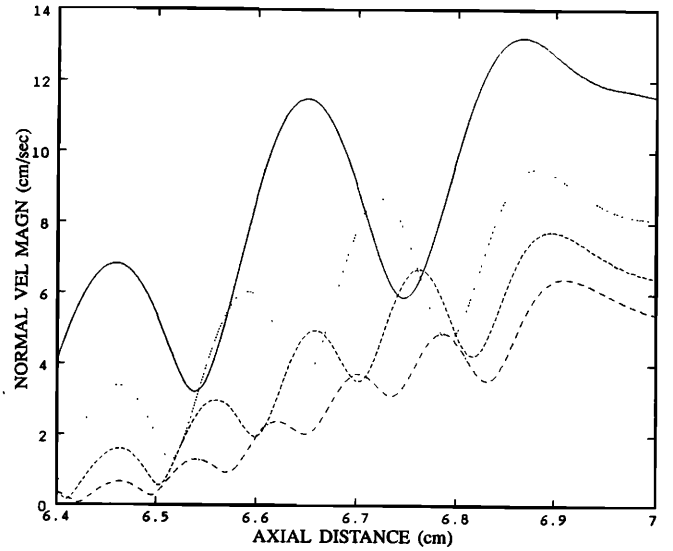


FIG. 19. Prefocal region complexity of the 30-W/cm$^2$ field. The 20th, 30th, 40th, and 50th harmonic axial amplitudes from $z = 6.4$ to $z = 7$ cm.

to the onset of focal nonlinear steepening (compare with axial harmonic amplitudes depicted in Fig. 15). Figure 14 is an overlay of the axial waveforms at $z = 9.9$ cm (in water) and at $z = 10.5$ cm (0.5 cm into the fat layer). Note the big drop in amplitude from the water shockwave. Finally, Fig. 15 shows the axial harmonic amplitudes with their rapid decline visible in the fat layer. One example in which an ultrasound scan could behave in an analogous manner is when a fetus is imaged through the lightly attenuating bladder and amniotic fluid. Potentially significant heating cases such as this can be examined with the model.

The phenomenon of beam broadening[7] associated with nonlinear effects and increasing source amplitudes has also been examined using the model. Using the same 3-MHz focused piston transducer and a medium of water the fields associated with source amplitudes of 3, 10, and 30 W/cm$^2$ were computed. The runs utilized 50 harmonics with an excess attenuation factor $q$ of 0.35, 50 harmonics with a $q$ of 0.5, and 70 harmonics with a $q$ of 0.4, respectively. The corresponding fundamental harmonic axial amplitudes are shown overlayed in Fig. 16(a). Note the loss of gain in the focal region amplitudes of the fundamental at the higher source intensities due to nonlinear losses. The corresponding second harmonic axial amplitudes are shown overlayed in Fig. 16(b). Note the shift in the position of the last axial minimum as the source amplitude is increased. This shift is clearly visible in the overlay of the second harmonic amplitudes [Fig. 16(b)] and barely visible in the overlay of the fundamental amplitudes [Fig. 16(a)]. An overlay of the focal plane ($z = 10$ cm) fundamental harmonic profiles is depicted in Fig. 17(a). Note the loss in nodal depth associated with increasing nonlinear effects and also the slight shift radially outward (broadening) of the corresponding nodes.

A more dramatic depiction of this nonlinearly generated broadening and distortion of the harmonic profiles is shown in Fig. 17(b). Here the corresponding fourth harmonic am-

plitude profiles are overlayed. Initially, the nodal depth increases near the axis as the source amplitude goes from 3–10 W/cm$^2$, then it decreases as the source amplitude goes up to 30 W/cm$^2$. Near the axis, the increased source amplitude produces increasing nodal shifts. Far off-axis though, the nodes remain aligned at all three source amplitudes. At intermediate radial distances there are bulges or shoulders in the profiles of the 10 and 30 W/cm$^2$ fourth harmonic amplitudes. These are located at about $r = 0.5$ cm and $r = 0.7$ cm, respectively. These shoulder regions represent the intersection of the near axis, broadened portion of the profile with the far off-axis, unshifted portion of the profile.

Figure 18(a)–(c) depict the first four harmonic, focal plane amplitude profiles of the 3, 10, and 30 W/cm$^2$ field propagations, respectively. The progressive broadening of the mainlobe can be seen clearly, especially amongst the higher harmonics. Finally, Fig. 19 highlights the prefocal region complexity of the 30-W/cm$^2$ field. Figure 19 depicts the 20th, the 30th, the 40th, and the 50th harmonic axial amplitude from $z = 6.4$ to $z = 7$ cm.

## VI. CONCLUSIONS

A new model for the nonlinear propagation of diffractive acoustic fields has been presented. The model explicitly accounts for the directionality of the field at each point and is not restricted to the established parabolic wave approximation to diffraction. In the case of propagation through multiple parallel layers of fluid medium, the model accounts for the effects of refraction and reflection (but not multiple reflections). Usage of a harmonic-limiting scheme with the frequency domain solution to Burgers' equation allows for the computation of some high-intensity shocked fields. The model also computes the spatial heating rate associated the field's absorption. Further work is planned in extending the implementation of the model to handle nonradially symmetric sources, in examining the possibility of deleterious tissue heating associated with clinical imaging, and in considering the performance of commercial ultrasonic medical devices including lithotripters.

## ACKNOWLEDGMENTS

The support, encouragement, and insightful advice from Professor E. L. Carstensen and Professor D. T. Blackstock are gratefully acknowledged. This work was supported in part by NIH Grant Nos. CA-39271 and DK-39796.

[1] David T. Blackstock, "Connection between the Fay and Fubini solutions for plane sound waves of finite amplitude," J. Acoust. Soc. Am. **39**, 1019–1026 (1966).

[2] M. F. Hamilton, "Fundamentals and applications of nonlinear acoustics," in *Nonlinear Wave Propagation in Mechanics*, edited by T. W. Wright (ASME, New York, 1985) AMD-Vol. 77.

[3] R. T. Beyer (Ed.), *Nonlinear Acoustics in Fluids* (Van Nostrand and Reinhold, New York, 1984).

[4] Carl W. Smith and Robert T. Beyer, "Ultrasonic radiation field of a focusing spherical source at finite amplitudes," J. Acoust. Soc. Am. **46**, 808–813 (1969).

[5] A. M. Sutin, "Influence of nonlinear effects on the properties of acoustic focusing systems," Sov. Phys. Acoust. **24**(4), 334–339 (1978).

[6] N. S. Bakhvalov, Y. A. M. Zhileikin, E. A. Zabolotskaya, and R. V. Khokhlov, "Focused high-amplitude sound beams," Sov. Phys. Acoust. **24**(1), 10–15 (1978).

[7] J. C. Lockwood, T. G. Muir, and D. T. Blackstock, "Directive harmonic generation in the radiation field of a circular piston," J. Acoust. Soc. Am. **53**, 1148–1153 (1973).

[8] Sigurd I. Aanonsen, T. Barkve, Jaqueline N. Tjøtta, and Sigve Tjøtta, "Distortion and harmonic generation in the nearfield of a finite amplitude sound beam," J. Acoust. Soc. Am. **75**, 749–768 (1984).

[9] Mark F. Hamilton, Jacqueline N. Tjøtta, and Sigve Tjøtta, "Nonlinear effects in the farfield of a directive sound source," J. Acoust. Soc. Am. **78**, 202–216 (1985).

[10] Bernard G. Lucas and Thomas G. Muir, "Field of a finite amplitude focusing source," J. Acoust. Soc. Am. **74**, 1522–1528 (1983).

[11] Jacqueline N. Tjøtta and Sigve Tjøtta, "Sound field of a parametric focusing source," J. Acoust. Soc. Am. **75**, 1392–1394 (1984).

[12] G. Du and M. A. Breazeale, "Theoretical description of a focused Gaussian ultrasonic beam in a nonlinear medium," J. Acoust. Soc. Am. **81**, 51–57 (1987).

[13] G. Du and M. A. Breazeale, "Harmonic distortion of a finite amplitude Gaussian beam in a fluid," J. Acoust. Soc. Am. **80**, 212–216 (1986).

[14] D. R. Bacon, "Finite amplitude distortion of the pulsed fields used in diagnostic ultrasound," Ultrasound Med. Biol. **10**(2), 189–195 (1984).

[15] D. R. Bacon, "Finite amplitude propagation in acoustic beams," Ph.D. thesis, University of Bath, 1986.

[16] T. S. Hart and M. F. Hamilton, "Nonlinear effects in focused sound fields," J. Acoust. Soc. Am. **84**, 1488–1496 (1988).

[17] T. S. Hart, "Numerical investigation of nonlinear effects in focused sound beams," M. S. thesis, U. Texas, Austin, 1987.

[18] H. F. Johnson, "An improved method for computing a discrete Hankel transform," Comp. Phys. Comm. **43**, 181–202 (1987).

[19] P. T. Christopher and K. J. Parker, "New approaches to the linear propagation of acoustic fields," J. Acoust. Soc. Am. **90**, 507–521 (1991).

[20] A. Korpel, "Frequency approach to nonlinear dispersive waves," J. Acoust. Soc. Am. **67**, 1954–1958 (1980).

[21] M. E. Haran and B. D. Cook, "Distortion of finite amplitude ultrasound in lossy media," J. Acoust. Soc. Am. **73**, 774–779 (1983).

[22] D. H. Trivett and A. L. Van Buren, "Comments on "Distortion of finite amplitude ultrasound in lossy media," J. Acoust. Soc. Am. **76**, 1257–1258 (1984).

[23] P. T. Christopher, "Developments in shockwave propagation using the frequency domain solution to Burgers' equation," J. Acoust. Soc. Am. (submitted) (1990).

[24] F. M. Pestorius, "Propagation of plane acoustic noise of finite amplitude," Tech. Rep. ARL-TR-73-23, Applied Research Laboratories, Univ. of Texas at Austin, AD 778–868 (1973).

[25] F. M. Pestorius and D. T. Blackstock, "Propagation of finite amplitude noise," in *Finite-Amplitude Wave Effects in Fluids: Proceedings of the 1973 Symposium, Copenhagen*, edited by L. Bjorno (IPCC Science and Technology Press, Ltd., Guilford, England, 1974), pp. 24–29.

[26] W. L. Nyborg, "Heat generation by ultrasound in a relaxing medium," J. Acoust. Soc. Am. **70**, 310–312 (1981).

[27] A. C. Baker, K. Anastasiadis, and V. F. Humphrey, "The nonlinear pressure field of a plane circular piston: Theory and experiment," J. Acoust. Soc. Am. **84**, 1483–1487 (1988).

[28] M. E. Lyons and K. J. Parker, "Absorption and attenuation in soft tissues II—experimental results," IEEE Trans. Ultra. Ferr. Freq. Cont. **35**(4), 511–521 (1988).

[29] S. A. Goss, R. L. Johnston, and F. Dunn, "Compilation of empirical ultrasonic properties of mammalian tissues. II.," J. Acoust. Soc. Am. **68**, 93–108 (1980).

[30] W. K. Law, L. A. Frizzell, and F. Dunn, "Determination of the nonlinearity parameter $B/A$ of biological media," Ultrasound Med. Biol. **11**(2), 307–318 (1985).